ELSEVIER

15 March 1998

OPTICS COMMUNICATIONS

Optics Communications 148 (1998) 300–315

Full length article

On the general properties of polarised light conventional and confocal microscopes

P. Török [1], P.D. Higdon, T. Wilson

Department of Engineering Science, University of Oxford, Parks Road, Oxford OX1 3PJ, UK

Received 12 June 1997; accepted 30 September 1997

Abstract

This paper considers the general properties of polarising microscopes and, in particular, light polarisation changes produced by high aperture lenses. A method is suggested for vectorial ray tracing of complex optical systems and to model high aperture lenses. The two principal arrangements of polarising microscopes (linearly and circularly polarised) are also considered. We discuss the effect of pinhole size on the detected intensity. A theory for point resolution of these microscopes is also presented and results are analysed. We support our theoretical predictions with experimental data.

Keywords: Diffraction; High-aperture; Focusing; Vectorial theory; Scanning optical microscopy; Confocal microscopy

1. Introduction

Polarised light microscopes are used in a wide variety of scientific disciplines ranging from minerology to the imaging of biological tissues. The basic theory of these instruments was first described by Inoué [1], Inoué and Hyde [2] and Kubota and Inoué [3] who found that an inevitable consequence of the image formation properties of these instruments was the presence of a "diffraction anomaly" which resulted in a finite extinction coefficient even if perfect polarising elements were used. It has recently been shown, however, that the confocal polarised light microscope does not suffer from this disadvantage and an infinite extinction ratio is predicted in the presence of perfect polars and an ideal point detector [4]. The use of a non-ideal finite sized (incoherent) pinhole detector, of course results in a finite value of extinction coefficient whereas the value always remains infinite if a coherent detector, such as a single mode optical fibre, is used [5,6].

The previous work on confocal polarisation microscopy has considered reflection systems and has ignored the polarisation changes caused by the use of high aperture microscope objectives. In this paper we extend this previous work by considering a transmission system with finite sized coherent and incoherent detectors. We introduce a model of high aperture objective lenses which is capable of describing the phase and amplitude modulation of light as it propagates through the lens. We elect to consider a transmission type microscope because it is the simplest set-up that can be characterised by itself, i.e. without the need for involving any specimen that would modify the transmittance of polarisation state of the light. We show, however, that a reflective specimen in, for example, a reflection type microscope would result in mathematical formulae which treat the material properties of the specimen separately from that of the microscope. We also obtain expressions for the field in the back focal plane of the second lens and compare it, in a pictorial format, to those obtained experimentally.

Analytical formulae are obtained for the field at the detector plane and differently sized coherent (i.e. sensitive to the electric field) and incoherent (i.e. sensitive to the intensity) detectors are considered. For polarising microscopes employing coherent detection we find the the detected signal level is identical for both the linearly and

[1] E-mail: peter.torok@eng.ox.ac.uk

PII S0030-4018(97)00576-2

circularly polarised cases, and further that the extinction ratio only depends on the quality of the polarisers. For incoherent detection the detected signal is affected by both the quality of the polarisers and the lenses, but even with perfect polarisers it is not possible to achieve infinite extinction when finite-sized detectors are used.

The properties of high numerical aperture lenses to effect polarisation are included in the theory for imaging point scatterers with polarised microscopes. We show simulated images of point scatterers for a linearly polarised microscope and for coherent and incoherent detection. Our results confirm that coherent detection results in a four-leaf pattern and incoherent detection results in a one-fold symmetry distribution [7].

Finally, we present experimental results that support our theoretical predictions, and draw our conclusions.

2. Transmission of light through high aperture optical systems – the concept of vectorial ray-tracing

The idea of vectorial ray-tracing was conceived a long time ago and used by, for example, Richards and Wolf [8]. The possibility to write matrices of vectorial ray-tracing was put forward by Török et al. [9] and then used by, for example, Török and Wilson [10] and Török et al. [11]. In this section we present the concept for vectorial ray-tracing by introducing the generalised form of Jones matrices. Throughout this section we shall assume [8] that the electric vector both maintains its direction with respect to a meridional plane and remains on the same side of a meridional plane on passing through the system. We also assume that there are no skew rays present in our optical system.

The Jones matrices are well-known [12] and readily available for the description of the state of polarisation as light traverses an optical system, but they are inherently not capable of describing non-collimated beams. This is because the Jones matrices are 2×2 in dimension. The matrices for vectorial ray-tracing of Török et al. [9] are 3×3 in dimension so that they are capable of describing non-collimated beams as well as collimated ones.

We now introduce the definition of *generalised Jones matrices*. We start by stating that when an oblique light ray is incident upon, say, a polariser then its propagation direction does not change after passing through the polariser (whose two surfaces are parallel to each-other) apart from a parallel shift with respect to the incident ray. It is thus possible to resolve the incident electric vector into components that are parallel and perpendicular to the surface of the polariser. Clearly, when the incident ray is perpendicular to the surface then no perpendicular electric vector component is created because the electric vector must be perpendicular to the direction of propagation. Since we find experimentally that there is no change in the direction of propagation of a light ray (i.e. the unit vector of propagation is not modified) this can only be possible if the polariser does not affect the perpendicular component of the electric field vector. This argument can readily be extended to all polarising devices that consist of two parallel surfaces (such as waveplates, Babinet-Soleil compensator, etc.).

We now suggest the following model of high aperture lens. These lenses consist of many individual lenses, for example a conventional microscope objective lens may contain as many as 10–15 individual elements and hence it is unlikely that we would be able to make general remarks by a detailed analysis of light propagation through all those surfaces. In order to be able to describe an arbitrary lens we have to find two functions, one describing the amplitude transmittance of the lens (the apodisation) and another describing the phase transmittance of the lens. The combination of these two functions will represent the microscope objective lens mathematically.

Lenses fundamentally are phase front converters; they are designed to convert either a plane or a spherical wavefront to a spherical or a plane phase front. Our present interest is to model a focusing type lens that converts a plane phase front into a perfectly spherical phase front.

On the other hand, we know that high aperture lenses effect the polarisation of the light (see, e.g., the paper by Hardy and Treves [13]). These authors considered a glass lens with a front surface of an ellipsoid of revolution and assumed that when light traverses the interface between air and glass it suffers a polarisation dependent attenuation that can be described by the Fresnel transmission coefficients. In principle, as we have said, it would be possible to model a complex lens by considering the Fresnel amplitude transmission coefficients on each interface but this method would result in a fairly complicated mathematical treatment. Instead, we determine a *single* interface that can represent *all* surfaces of the objective lens. We find such an interface by fitting polynomials on the experimental back-aperture distributions and comparing them to theoretical predictions. Such comparisons show that a spherical surface describes our experimental results with the highest precision. It is, however, important to emphasise that this model does not mean that the objective lens is replaced by a spherical air/glass interface, but rather than the amplitude transmittance of the objective lens is modelled by a function that is determined from such considerations.

Notations in this paper are used such that electric vectors (i.e. strength vectors) are denoted by capital letters (e.g. $\boldsymbol{E}_n$) and electric *field* vectors are denoted by small letters (e.g. $\boldsymbol{e}_n$).

Now we continue by ray-tracing a high aperture optical system (see Fig. 1) by means of the generalised Jones matrices. We begin by considering a collimated beam that is linearly polarised in the x axis (see Fig. 1). The electric vector of illumination is then given by:

$$\boldsymbol{E}_0 = (1,0,0). \tag{1}$$

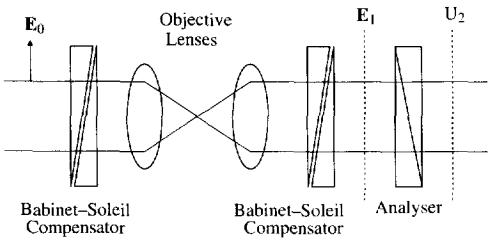

Fig. 1. Diagram for calculating the electric field vector $\boldsymbol{E}_1$ after the second Babinet-Soleil compensator.

It will be convenient to define a co-ordinate system with spherical polar co-ordinates r, θ and ϕ such that $r>0$, $0 \le \theta < \pi$ and $0 \le \phi < 2\pi$.

The electric vector after the second Babinet-Soleil compensator is given by

$$\boldsymbol{E}_1 = \mathbf{BS}_2 \cdot \mathbf{R}^{-1} \cdot \mathbf{L}^{-1} \cdot \mathbf{I}_2 \cdot \mathbf{R} \cdot \mathbf{R}^{-1} \cdot \mathbf{I}_1 \cdot \mathbf{L} \cdot \mathbf{R} \cdot \mathbf{BS}_1 \cdot \boldsymbol{E}_0, \tag{2}$$

where the matrix $\mathbf{R}$ describes the co-ordinate transformation for rotation around the z axis:

$$\mathbf{R} = \begin{pmatrix} \cos\phi & \sin\phi & 0 \\ -\sin\phi & \cos\phi & 0 \\ 0 & 0 & 1 \end{pmatrix}, \tag{3}$$

and the matrix $\mathbf{L}$ describes the changes in the electric field as it traverses the one of the objective lenses:

$$\mathbf{L} = \begin{pmatrix} \cos\theta & 0 & \sin\theta \\ 0 & 1 & 0 \\ -\sin\theta & 0 & \cos\theta \end{pmatrix}, \tag{4}$$

and the angle and polarisation dependent transmittance on the lens is described by the matrix $\mathbf{I}_n$ where $n = 1,2$ denotes the first and second objective lenses, respectively:

$$\mathbf{I} = \sqrt{\cos\theta} \begin{pmatrix} \tau_p & 0 & 0 \\ 0 & \tau_s & 0 \\ 0 & 0 & \tau_p \end{pmatrix}, \tag{5}$$

where we have introduced the term $\sqrt{\cos\theta}$ to account for an aplanatic lens and τ_p and τ_s are the Fresnel transmission coefficients [15]:

$$\tau_p = \frac{2\sin\theta_{II}\cos\theta_I}{\sin(\theta_I+\theta_{II})\cos(\theta_I-\theta_{II})}, \quad \tau_s = \frac{2\sin\theta_{II}\cos\theta_I}{\sin(\theta_I+\theta_{II})}, \tag{6}$$

where θ_I and θ_{II} represent the incident and refracted angles, respectively. Numerical values used in the above equations are given in Section 5.

The matrix **BS** denotes the generalised Jones matrix for the Babinet-Soleil compensator [12] and is given by:

$$\mathbf{BS}_n = \begin{pmatrix} A_n^+ & iB_n & 0 \\ iB_n & A_n^- & 0 \\ 0 & 0 & 1 \end{pmatrix}, \tag{7}$$

where

$$A_n^{\pm} = \cos\frac{\delta_n}{2} \pm i\cos 2\phi_{Bn}\sin\frac{\delta_n}{2}, \quad B_n = \sin\frac{\delta_n}{2}\sin 2\phi_{Bn}. \tag{8}$$

and ϕ_{Bn} denotes the orientation and δ_n the retardation of the Babinet-Soleil compensator and the matrix element (3,3) signifies that the Babinet-Soleil compensator does not modify the longitudinal component of the electric vector and n, again, indicates whether the first or second compensator is mentioned. We note that this matrix, just as others used in our formalism apart from $\mathbf{I}_n$, is unitary.

After some straightforward algebraic manipulation the electric field $\boldsymbol{E}_1$ is obtained as:

$$\boldsymbol{E}_1 = \begin{pmatrix} A_1^+A_2^+C - B_1B_2D + i(B_1A_2^+ + B_1B_2)T^-\sin 2\phi \\ (A_1^+A_2^- - B_1B_2)T^-\sin 2\phi + i(B_1A_2^-D + A_1^+B_2C) \\ 0 \end{pmatrix}, \tag{9}$$

where

$$C = T^+ + T^-\cos 2\phi, \quad D = T^+ - T^-\cos 2\phi.$$

In the above expression we have used the following substitution:

$$T^+ = (\tau_{p1}\tau_{p2} + \tau_{s1}\tau_{s2})\cos\theta, \quad T^- = (\tau_{p1}\tau_{p2} - \tau_{s1}\tau_{s2})\cos\theta. \tag{10}$$

When the electric vector $\boldsymbol{E}_1$ is passed through an analyser then the resulting vectorial field is given by:

$$\boldsymbol{E}_2 = \mathbf{O}\,\boldsymbol{E}_1, \tag{11}$$

where

$$\mathbf{O} = \begin{pmatrix} \cos^2\gamma & \sin\gamma\cos\gamma & 0 \\ \sin\gamma\cos\gamma & \sin^2\gamma & 0 \\ 0 & 0 & 1 \end{pmatrix} \tag{12}$$

that is the generalised Jones matrix of a polariser whose axis makes an angle γ with the positive x direction.

Because of the form of Eq. (9), when the electric *vector* is converted to a *scalar* quantity we may use the following expression:

$$U_2 = \mathbf{S}\,\boldsymbol{E}_2, \tag{13}$$

where

$$\mathbf{S} = (1,1,1). \tag{14}$$

Eq. (9) represents the electric vector in the back focal plane of the right-hand-side objective lens. It is of particular interest to determine the intensity in this plane when the Babinet-Soleil compensators are set to zero retardation ($\delta_n = 0$) so producing a linearly polarised configuration. For this case

$$\mathbf{BS}_1 = \mathbf{BS}_2 = \begin{pmatrix} 1 & 0 & 0 \\ 0 & 1 & 0 \\ 0 & 0 & 1 \end{pmatrix} \tag{15}$$

that is a unit matrix. The analyser after the second Babinet-Soleil compensator is set at an angle γ with respect to the direction of incident polarisation and hence we obtain from Eq. (13):

$$\boldsymbol{E}_1 = \begin{pmatrix} T^+ + T^- \cos 2\phi \\ T^- \sin 2\phi \\ 0 \end{pmatrix}, \tag{16}$$

which leads to the intensity $I_2^{\delta=0}$ after the analyser (Fig. 1):

$$\begin{aligned} I_2^{\delta=0} &= |U_2^{\delta=0}|^2 \\ &= |g(\gamma)|^2 |\cos\gamma\,(T^+ + T^- \cos 2\phi) \\ &\quad + \sin\gamma\,(T^- \sin 2\phi)|^2, \end{aligned} \tag{17}$$

where $g(\gamma) = \sin\gamma + \cos\gamma$. In the above expression the superscript $\delta = 0$ indicates that this intensity distribution is only applicable to zero retardation setting of the Babinet-Soleil compensators.

Eq. (17) represents the intensity in the back focal plane of the second objective lens when the analyser is set to an angle γ with respect to the incident polarisation. We have used this formula to compute the intensity for different analyser directions. These results are presented in Section 6.

It is interesting to note that for a reflection type microscope the material properties of the reflective specimen may be readily included because it is treated as part of the apodisation function. To show this we write the electric vector $\boldsymbol{E}_R$ before the analyser for a linearly polarised reflection type microscope by:

$$\boldsymbol{E}_R = \mathbf{R}^{-1}\mathbf{L}^{-1}\mathbf{I}_2\mathbf{P}^{-1}\mathbf{I}_R\mathbf{P}\mathbf{I}_1\mathbf{L}\mathbf{R}\,\boldsymbol{E}_0, \tag{18}$$

where $\mathbf{I}_R$ is the matrix for the reflection given by:

$$\mathbf{I}_R = \begin{pmatrix} r_p & 0 & 0 \\ 0 & -r_s & 0 \\ 0 & 0 & r_p \end{pmatrix}, \tag{19}$$

where r_p and r_s are the Fresnel reflection coefficients and

$$\mathbf{P} = \begin{pmatrix} \cos\theta & 0 & -\sin\theta \\ 0 & 1 & 0 \\ \sin\theta & 0 & \cos\theta \end{pmatrix}. \tag{20}$$

It is not difficult to show that Eq. (18) results in:

$$\boldsymbol{E}_R = \begin{pmatrix} K^- + K^+ \cos 2\phi \\ K^+ \sin 2\phi \\ 0 \end{pmatrix}, \tag{21}$$

where

$$\begin{aligned} K^+ &= (\tau_{p1}\tau_{p2}r_p + \tau_{s1}\tau_{s2}r_s)\cos\theta, \\ K^- &= (\tau_{p1}\tau_{p2}r_p - \tau_{s1}\tau_{s2}r_s)\cos\theta. \end{aligned} \tag{22}$$

The above equation shows that material dependent properties of both the lenses and the reflective specimen are included in functions $K^\pm$ that are independent of any parameter of the microscope. We note that these expressions reduce to those of Wilson and Tan [5] when the effect of the lens on polarisation is ignored.

3. Theory of polarising microscopes

Now we continue our investigations by considering the general form of the field that is produced by a lens (the so-called detector lens) placed at a distance f from the plane of analyser (f being the focal length of the detector lens). The numerical aperture of the detector lens is, in the practice, very low (< 0.1). This optical set-up is a true Fourier transforming arrangement [16] and hence the scalar field in the focal plane of the detector lens is given by (Fig. 2) the truncated Fourier transform of the scalar field U_2:

$$\begin{aligned} U_3(\rho, \phi_p; \gamma) = \int_0^{\alpha_2}\int_0^{2\pi} U_2(\theta_2, \phi; \gamma) \sin 2\theta_2 \\ \times \exp\left[ik\rho \sin\theta_2 \cos(\phi - \phi_p)\right] \mathrm{d}\theta_2\, \mathrm{d}\phi. \end{aligned} \tag{23}$$

The scalar field U_2 is given from Eq. (13) by:

$$U_2 = M_1 T^+ + M_2 T^- \cos 2\phi + M_3 T^- \sin 2\phi, \tag{24}$$

where we have introduced:

$$\begin{aligned} M_1 &= g(\gamma)\left[(A_1^+ A_2^+ - B_1 B_2)\cos\gamma \right. \\ &\quad \left. + i(B_1 A_2^- + A_1^+ B_2)\sin\gamma\right], \\ M_2 &= g(\gamma)\left[(A_1^+ A_2^+ + B_1 B_2)\cos\gamma \right. \\ &\quad \left. - i(B_1 A_2^- - A_1^+ B_2)\sin\gamma\right], \\ M_3 &= g(\gamma)\left[(A_1^+ A_2^- - B_1 B_2)\sin\gamma \right. \\ &\quad \left. + i(B_1 A_2^+ + B_1 B_2)\cos\gamma\right], \end{aligned} \tag{25}$$

and we note that

$$M_n = f(\phi_{B1}, \delta_{B1}; \phi_{B2}, \delta_{B2}; \gamma), \tag{26}$$

which means that all polarisation components of the optical system are transformed into the functions M_n and

$$T^\pm = f(\theta_1, \theta_2) \tag{27}$$

Having obtained the scalar field after the analyser we

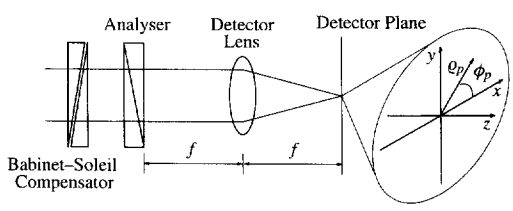

Fig. 2. Diagram showing the detector lens arrangement.

proceed to derive the scalar field U_3 in the detector plane. From Eqs. (23) and (24) we have:

$$U_3 = M_1 \int_0^{\alpha_2} T^+ J_0(k\rho\sin\theta_2)\sin 2\theta_2 \, \mathrm{d}\theta_2 - \left(M_2 \cos 2\phi_p + M_3 \sin 2\phi_p\right) \times \int_0^{\alpha_2} T^- J_2(k\rho\sin\theta_2)\sin 2\theta_2 \, \mathrm{d}\theta_2, \tag{28}$$

where we have used the identity [14]:

$$\int_0^{2\pi} \begin{matrix}\cos n\theta \\ \sin n\theta\end{matrix} \exp[i\rho\cos(\theta-\zeta)]\,\mathrm{d}\theta = 2\pi i^n J_n(\rho) \begin{matrix}\cos n\zeta \\ \sin n\zeta\end{matrix} \tag{29}$$

and $J_n(\,)$ is the Bessel function of zero kind, order n.

Eq. (28) constitutes the general solution for a polarised microscope consisting of two, arbitrary aligned Babinet-Soleil compensators, two objective lenses and an analyser.

A detector placed in the focal plane of the detector lens can either be sensitive to the intensity or the field present in the focal plane. According to this we distinguish between incoherent and coherent detectors. We shall now discuss both of these detections.

3.1. Incoherent detection

When an incoherent detector is employed then the intensity in the focal plane is detected (Fig. 2):

$$I = \int_D |U_3|^2 S_D \, \mathrm{d}D = \int_0^R \int_0^{2\pi} |U_3|^2 f(\rho)\rho \, \mathrm{d}\rho \, \mathrm{d}\phi_p, \tag{30}$$

where S_D is the sensitivity function and D is the area of the detector, or for a rotationally symmetrical detector R is the radius and $f(\rho)$ is the sensitivity function of the detector. Since

$$|U_3|^2 = U_3 U_3^*, \tag{31}$$

where $*$ denotes the complex conjugation. From Eqs. (28) and (30) we obtain:

$$I = 2|M_1|^2 \int_0^R P_0^2 \rho \, \mathrm{d}\rho + \left(|M_2|^2 + |M_3|^2\right) \int_0^R P_2^2 \rho \, \mathrm{d}\rho, \tag{32}$$

where we have introduced

$$P_0 = \int_0^{\alpha_2} T^+ J_0(k\rho\sin\theta_2)\sin 2\theta_2 \, \mathrm{d}\theta_2,$$

$$P_2 = \int_0^{\alpha_2} T^- J_2(k\rho\sin\theta_2)\sin 2\theta_2 \, \mathrm{d}\theta_2, \tag{33}$$

and set $f(\rho) = 1$. For a non-absorbing lens $\Im\{T^{\pm}\} = 0$ and hence $\Im\{P_n\} = 0$, that is to say functions P_0 and P_2 are purely real. We note that if we assume ideal lenses, i.e. lenses that do not affect the polarisation of the light, we take $\tau_p = \tau_s = 1$ and hence $T^+ = 2\cos\theta$ and $T^- = 0$, from which $P_2 = 0$. In this case

$$I = 2|M_1|^2 \int_0^R P_0^2 \rho \, \mathrm{d}\rho. \tag{34}$$

3.2. Coherent detection

When a coherent detector (such as a single mode optical fibre) is employed the detection is sensitive to the field rather than the intensity:

$$I = \left| \int_D U_3 S_D \, \mathrm{d}D \right|^2 = \left| \int_0^R \int_0^{2\pi} U_3 f(\rho)\rho \, \mathrm{d}\rho \, \mathrm{d}\phi_p \right|^2, \tag{35}$$

which gives from Eq. (28), after integration by ϕ_p:

$$I = \left| \int_0^R \int_0^{\alpha_2} M_1 T^+ f(\rho) J_0(k\rho\sin\theta_2)\sin 2\theta_2 \, \rho \, \mathrm{d}\rho \, \mathrm{d}\theta_2 \right|^2. \tag{36}$$

The above equation can analytically be evaluated for two special cases. First we consider an infinitely large detector with a Gaussian sensitivity function:

$$R \to \infty, \quad f(\rho) = \exp\left(-\frac{\rho^2}{b^2}\right), \tag{37}$$

for which we have

$$\int_0^{\infty} J_0(k\rho\sin\theta_2)\exp\left(-\frac{\rho^2}{b^2}\right)\rho \, \mathrm{d}\rho = \frac{b^2}{2}\exp\left(-\frac{b^2 k^2 \sin^2\theta_2}{4}\right) = S_1(\theta_2). \tag{38}$$

We note that this case corresponds to having a single mode optical fibre detector, if the value of b is selected such that the Gaussian function produces sufficiently small value at lateral sizes greater than the radius of the fibre.

The other case is when the radius of the detector is finite and its sensitivity function is unity:

$$R \to R, \quad f(\rho) = 1, \tag{39}$$

that yields:

$$\int_0^R J_0(k\rho\sin\theta_2)\rho \, \mathrm{d}\rho = \frac{R}{k\sin\theta_2} J_1(Rk\sin\theta_2) = S_2(\theta_2). \tag{40}$$

Finally, the detector signal for the coherent case is given by:

$$I = \left| M_1 \int_0^{\alpha_2} T^+ \sin 2\theta_2 S_n(\theta_2) \, \mathrm{d}\theta_2 \right|^2. \tag{41}$$

In Eq. (41) the integral term is constant when a fibre optics detector is used.

4. Theory of polarising microscopes imaging point scatterers

In the previous sections we have derived the theory of polarising microscopes when no specimen is employed. This was clearly essential to gain an understanding of the operation of the microscope. It is, however, frequently the case that optical microscopes are quantified by obtaining their response to a point object. Polarising microscopes can only be described mathematically by considering the vectorial nature of light and hence the closest equivalent of a point object in polarisation microscopy is a point scatterer. Wilson et al. [7] have already considered the image of a sub-resolution dielectric point scatterer in a reflection geometry and for an infinitely small pinhole. In the following we shall both extend their analysis to the transmission case, include the effect of the high aperture microscope lenses on polarisation and include the case of a finite sized detector. We shall again use the vectorial ray tracing approach.

Following the principles of Wilson et al. [7] and Török et al. [11] we assume that when the point dielectric scatterer is so small that its far field is identical to that produced by an electric dipole whose dipole moment $\boldsymbol{p}$ is proportional to the incident electric field. We also assume that no magnetic coupling occurs. Hence the electric field in the radiation zone of the dielectric scatterer is given by:

$$\boldsymbol{E}_{dp} = -\boldsymbol{r}\times(\boldsymbol{r}\times\boldsymbol{p}). \tag{42}$$

The illumination of the scatterer occurs by the first objective lens whose electric vector $\boldsymbol{E}'_{dp}$ in the vicinity of the focus is given by

$$\boldsymbol{E}'_{dp} = \mathbf{R}^{-1}\mathbf{I}_1\mathbf{L}\,\mathbf{R}\,\boldsymbol{E}_0, \tag{43}$$

that gives for the Cartesian components of the electric vector:

$$\begin{aligned}
E_{dp,x} &= \cos^{1/2}\theta_1\left[\tfrac{1}{2}(\tau_p\cos\theta_1) + \tfrac{1}{2}(\tau_p\cos\theta_1 - \tau_s)\cos 2\phi\right],\\
E_{dp,y} &= \cos^{1/2}\theta_1\,\tfrac{1}{2}(\tau_p\cos\theta_1 - \tau_s)\sin 2\phi,\\
E_{dp,z} &= -\cos^{1/2}\theta_1\,\tau_p\sin\theta\cos\phi.
\end{aligned} \tag{44}$$

The electric field is then given by the integral formula of Richards and Wolf [8] transformed into spherical polar co-ordinates (Fig. 3):

$$\begin{aligned}
\boldsymbol{e}_{dp} = \int_0^{\alpha_1}\int_0^{2\pi}&\boldsymbol{E}_{dp}(\phi,\theta_1)\exp(ikz_s\cos\theta_1)\\
&\times\exp\left[ik\rho_s\sin\theta_1\cos(\phi-\phi_p)\right]\sin\theta_1\,\mathrm{d}\theta_1\,\mathrm{d}\phi,
\end{aligned} \tag{45}$$

from which we obtain the Cartesian components of the electric field:

$$\begin{aligned}
&e_{dp,x} = \pi(I_0 - I_2\cos 2\phi_s), \quad e_{dp,y} = \pi I_2\sin 2\phi_s,\\
&e_{dp,z} = -2i\pi I_1\cos\phi_s,
\end{aligned} \tag{46}$$

where we have ignored constant multipliers and

$$\begin{aligned}
I_0(\rho_s,z_s) &= \int_0^{\alpha_1}\sqrt{\cos\theta_1}\,(\tau_p\cos\theta_1 + \tau_s)\\
&\quad\times\sin\theta_1 J_0(k\rho_s\sin\theta_1)\exp(ikz_s\cos\theta)\,\mathrm{d}\theta_1,\\
I_1(\rho_s,z_s) &= \int_0^{\alpha_1}\sqrt{\cos\theta_1}\,\tau_p\sin^2\theta_1 J_1(k\rho_s\sin\theta_1)\\
&\quad\times\exp(ikz_s\cos\theta)\,\mathrm{d}\theta_1,\\
I_2(\rho_s,z_s) &= \int_0^{\alpha_1}\sqrt{\cos\theta_1}\,(\tau_p\cos\theta_1 - \tau_s)\\
&\quad\times\sin\theta_1 J_2(k\rho_s\sin\theta_1)\exp(ikz_s\cos\theta)\,\mathrm{d}\theta_1.
\end{aligned} \tag{47}$$

Hence the Cartesian components of the dipole moment are given by:

$$p_x = I_0 - I_2\cos 2\phi_s, \quad p_y = I_2\sin 2\phi_s, \quad p_z = -2iI_1\cos\phi_s. \tag{48}$$

In the linearly polarised transmission microscope the second objective lens images the far-field irradiation of the scatterer. Before we proceed with the mathematics it is worth pointing out what the conditions are under which our approach is valid. We shall assume in the following that the scatterer is located in the vicinity of the focus. We make this restriction in the lateral direction to avoid off-axis aberrations and in the axial direction to avoid aberrations associated with tube-length correction. We note that it is not necessary to make this restriction to the axial direction, as shown by Török et al. [11], but here we do make this restriction in order to ease the mathematics.

The electric vector $\boldsymbol{E}_2$, after being collimated by the second objective lens, is given by (Fig. 4) :

$$\boldsymbol{E}_2 = \mathbf{R}^{-1}\mathbf{L}^{-1}\mathbf{I}_2\mathbf{R}\,\boldsymbol{E}'_{dp}, \tag{49}$$

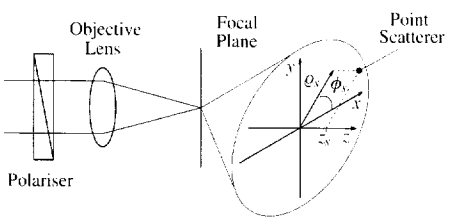

Fig. 3. Schematic diagram for the calculation of imaging a point scatterer.

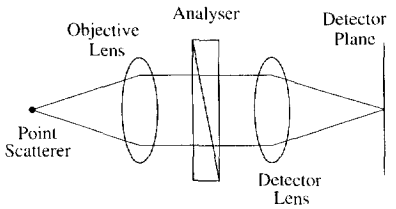

Fig. 4. Diagram for calculating the detector signal from a point scatterer

that leads to the Cartesian components of the electric vector:

$$
\begin{aligned}
E_{2x} &= \cos^{1/2}\theta_1\{p_x[(\tau_s+\tau_p\cos\theta_1)\\
&\quad -(\tau_s-\tau_p\cos\theta_1)\cos 2\phi]\\
&\quad -p_y(\tau_s-\tau_p\cos\theta_1)\sin 2\phi\\
&\quad -2p_z\tau_p\cos\phi\sin\theta_1\},\\
E_{2y} &= \cos^{1/2}\theta_1\{-p_x(\tau_s-\tau_p\cos\theta_1)\sin 2\phi\\
&\quad +p_y[(\tau_s+\tau_p\cos\theta_1)+(\tau_s-\tau_p\cos\theta_1)\cos 2\phi]\\
&\quad -2p_z\tau_p\sin\phi\sin\theta_1\},\\
E_{2z} &= 0. \qquad (50)
\end{aligned}
$$

This electric vector is then passed through an analyser which is located in the back focal plane of the detector lens. The detector lens hence produces the Fourier transform of the scalar field after the polariser to give the scalar field distribution in the detector plane:

$$
\begin{aligned}
U_p &= g(\gamma)[\cos\gamma p_x-\sin\gamma p_y]I_0^p\\
&\quad -2p_z ig(\gamma)[\cos\gamma\cos\phi_p+\sin\gamma\sin\phi_p]I_1^p\\
&\quad -g(\gamma)\{[\cos\gamma p_x-\sin\gamma p_y]\cos 2\phi_p\\
&\quad +[\cos\gamma p_y+\sin\gamma p_x)]\sin 2\phi_p\}I_2^p, \qquad (51)
\end{aligned}
$$

where $f(\gamma)=1+\sin 2\gamma+\cos 2\gamma$ and

$$
\begin{aligned}
I_0^p &= \int_0^{\alpha_2}\sqrt{\cos\theta_1}\,(\tau_s+\tau_p\cos\theta_1)\sin 2\theta_2 J_0(k\rho\sin\theta_2)\\
&\quad \times\exp(-ikz_s\cos\theta_1)\,\mathrm{d}\theta_2,\\
I_1^p &= \int_0^{\alpha_2}\sqrt{\cos\theta_1}\,\tau_p\sin\theta_1\sin 2\theta_2 J_1(k\rho\sin\theta_2)\\
&\quad \times\exp(-ikz_s\cos\theta_1)\,\mathrm{d}\theta_2,\\
I_2^p &= \int_0^{\alpha_2}\sqrt{\cos\theta_1}\,(\tau_s-\tau_p\cos\theta_1)\sin 2\theta_2 J_2(k\rho\sin\theta_2)\\
&\quad \times\exp(-ikz_s\cos\theta_1)\,\mathrm{d}\theta_2, \qquad (52)
\end{aligned}
$$

and we have introduced in this equation the phase term $\exp(-ikz_s\cos\theta_1)$ to account for the defocus of the scatterer. Note that the defocus is opposite in sign in Eq. (47) because of the transmission set-up.

It now remains to determine the detector signals when coherent and incoherent detectors are employed. For an incoherent detector the detected intensity is given by:

$$
\begin{aligned}
I_{\mathrm{inc}} &= \int_D |U_p(\boldsymbol{r}_p)|^2\,\mathrm{d}D\\
&= \int_0^R\int_0^{2\pi}|U_p(\boldsymbol{r}_d-\beta\boldsymbol{r}_s)|^2 r_d\,\mathrm{d}r_d\,\mathrm{d}\phi_d. \qquad (53)
\end{aligned}
$$

For a coherent detector the detected signal is given by:

$$
\begin{aligned}
I_{\mathrm{coh}} &= \left|\int_D U_p(\boldsymbol{r}_p)\,\mathrm{d}D\right|^2\\
&= \left|\int_0^R\int_0^{2\pi}U_p(\boldsymbol{r}_d-\beta\boldsymbol{r}_s)\,r_d\,\mathrm{d}r_d\,\mathrm{d}\phi_d\right|^2, \qquad (54)
\end{aligned}
$$

where we have ignored constant multipliers.

5. Numerical results

Numerical results are presented here for our experimental set-up (see Section 6 for a detailed description). In all numerical computations the following system parameters were used. The two objective lenses we used in numerical evaluation possessed a numerical aperture of 1.3 for oil immersion. The detector lens had a focal length of 100 mm and a light wavelength of $\lambda = 632.8$ nm was used. In Eq. (6) we took $n_1 = 1$, $n_2 = 1.54$ for the *first* lens and $n_1 = 1.54$, $n_2 = 1$ for the *second* lens. This we did because we model our lenses as spherical dielectric surfaces; for the first lens the light propagates from air to glass/immersion oil whilst for the second lens the light propagates from immersion oil/glass to air. These values were chosen mainly because they corresponded to the experimental condition, but also because theoretical predictions for the back focal plane distributions gave the best match with these values. Programs were written in C + + and Mathematica and run on a Sun workstation.

In the following we concentrate on the two special cases of polarised light microscopes, the linearly and the circularly polarised geometries. The intensity or the field in the detector plane plays an important role for an incoherent or a coherent detection, respectively. For linear polarisation and for the cross polarised case the intensity and the field are shown in Fig. 5. When an incoherent detector is employed in the detector plane then the intensity is detected and hence at larger detector sizes finite intensity readings are anticipated. When, however, a coherent detector is employed, which observes the field rather than the intensity, the figure clearly shows that zero detector signal is anticipated (as long as the detector is centered on the optical axis). For reference the white dashed circle in the Figure shows the first minimum (zero) of an Airy distribution. It is seen that cross polars produce considerably wider light distribution in the detector plane compared to that when the polars are parallel.

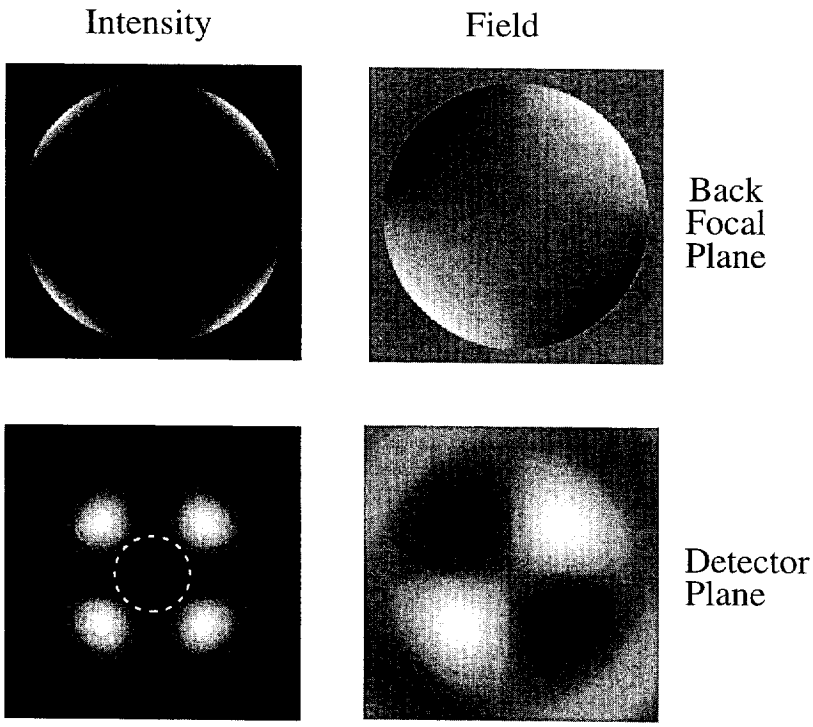

Fig. 5. Distributions of the intensity and the field for a linearly polarised microscope in the back focal plane of the second objective lens and in the detector plane. White dashed circle shows the first zero of the Airy distribution.

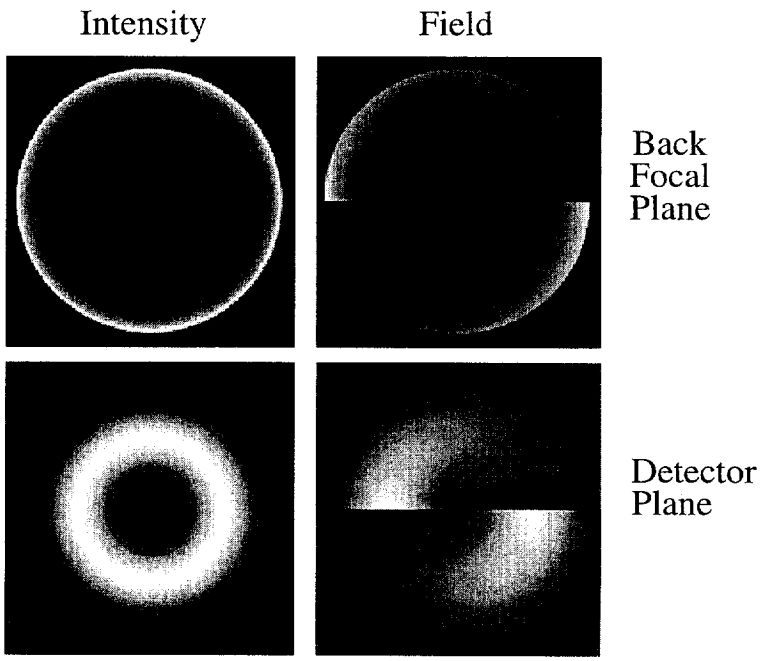

Fig. 6. Distributions of the intensity and the field for a circularly polarised microscope in the back focal plane of the second objective lens and in the detector plane.

For circularly polarised microscope the field and intensity in the back focal plane and in the detector plane is shown in Fig. 6. This situation emphasises the importance of the simultaneous study of the field and the intensity. If, for example, we wanted to determine the form of intensity distribution in the detector plane, just by considering the intensity in the back focal plane then an incorrect distribution would result because the phase of the field in the back focal plane, which rotates with 2ϕ would have been ignored. Fig. 6 also shows that when a coherent detector is employed (i.e. detecting the field) then the resulting detector signal will be zero. Conversely, for sufficiently large incoherent detectors the signal will be finite. The figure also suggests that we may anticipate zero signal for both coherent and small incoherent detectors.

5.1. Linearly polarised microscope

For the linearly polarised microscope we may write, from Eqs. (8) and (25):

$$A_n^{\pm} = 1, \quad \text{and} \quad B_n = 0,$$

$$M_1 = g(\gamma)\cos\gamma, \quad M_2 = g(\gamma)\cos\gamma, \quad M_3 = g(\gamma)\sin\gamma, \tag{55}$$

from which the general expression for the detector signal of a microscope using an incoherent detector the detected intensity is given by:

$$I = 2\cos^2\gamma \int_0^R P_0^2 \rho \, d\rho + \int_0^R P_2^2 \rho \, d\rho, \tag{56}$$

where the constant multipliers are ignored. The above equations permit us to estimate the detector signal for coherent and incoherent detectors for linear polarisation. When the polariser and the analyser are crossed the coherent detector signal will be zero and hence the extinction (defined by $I(\gamma = 0°)/I(\gamma = 90°)$) will be infinite. Is is important to emphasise that this is only the case when perfect polarisers are used. In practice good quality polarisers possess an extinction ratio of $\approx 10^5$ which is then the fundamental limit of linearly polarised microscopes employing coherent detection. Eq. (56) shows that for an incoherent detector, and for crossed polars, the detected intensity will always be finite, except for when infinitely small pinholes are applied. In this latter case, however, the detection approximates the coherent limit so zero detected signal is anticipated.

To examine the effect of microscope objective lens numerical aperture on the detected intensity we have computed the results shown in Fig. 7, that was computed from Eq. (56) using $R = 5$ μm. This figure shows that, as anticipated, high numerical aperture objective lenses affect the polarisation more and hence a worse detected intensity for analyser angles close to the crossed direction.

If we take $R \to 0$ in Eq. (56) then the second term becomes negligibly small and hence the first term dominates, resulting in a general $\cos^2\gamma$ dependence of the detected intensity.

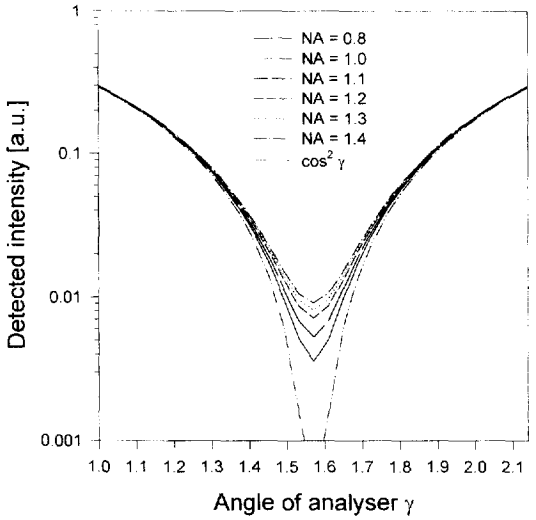

Fig. 7. Detected intensity as a function of analyser angle γ (in radians) for a linearly polarised microscope. The objective lens numerical aperture is the parameter.

5.2. Circularly polarised microscope

For the circularly polarised microscope ($\phi_{B1} = \phi_{B2} = \pi/4$, $\delta_1 = \pi/2$, $\delta_2 = -\pi/2$) we may write, from Eqs. (8) and (25):

$$A_n^{\pm} = \frac{1}{\sqrt{2}}, \quad B_1 = \frac{1}{\sqrt{2}}, \quad B_2 = -\frac{1}{\sqrt{2}},$$

$$M_1 = g(\gamma)\cos\gamma, \quad M_2 = -ig(\gamma)\sin\gamma,$$

$$M_3 = g(\gamma)\sin\gamma. \tag{57}$$

It is interesting to note that, as shown by Eqs. (55) and (57), parameter M_1 is the same for both the linearly and the circularly polarised microscopes. This means that the detected signal of a coherent microscope and for the circularly polarised case will be identical to that obtained for the linearly polarised case.

The incoherent detected intensity is given from Eqs. (56) and (57) by:

$$I = 2\cos^2\gamma \left[\int_0^R P_0^2 \rho \, d\rho - \int_0^R P_2^2 \rho \, d\rho \right] + 2\int_0^R P_2^2 \rho \, d\rho$$

$$= 2\left[\cos^2\gamma \int_0^R P_0^2 \rho \, d\rho + \sin^2\gamma \int_0^R P_2^2 \rho \, d\rho \right], \tag{58}$$

where the constant multipliers are ignored. The above equation shows that the detector signal for a circularly polarised microscope employing an incoherent detector will be finite for $\gamma = 90°$ except for, again, the case when small pinholes are used.

Table 1
Special cases for incoherent detector signal as a function of analyser angle γ

γ	Linear	Circular
0°	$\int_0^R (2P_0^2 + P_2^2)\rho\,d\rho$	$2\int_0^R P_0^2\rho\,d\rho$
45°	$\int_0^R (P_0^2 + P_2^2)\rho\,d\rho$	$\int_0^R (P_0^2 + P_2^2)\rho\,d\rho$
90°	$\int_0^R P_2^2\rho\,d\rho$	$2\int_0^I P_2^2\rho\,d\rho$

In Table 1 we compare the linear and circular cases for an incoherent detector to find that the detector signal for a linearly polarised microscope will somewhat be higher for

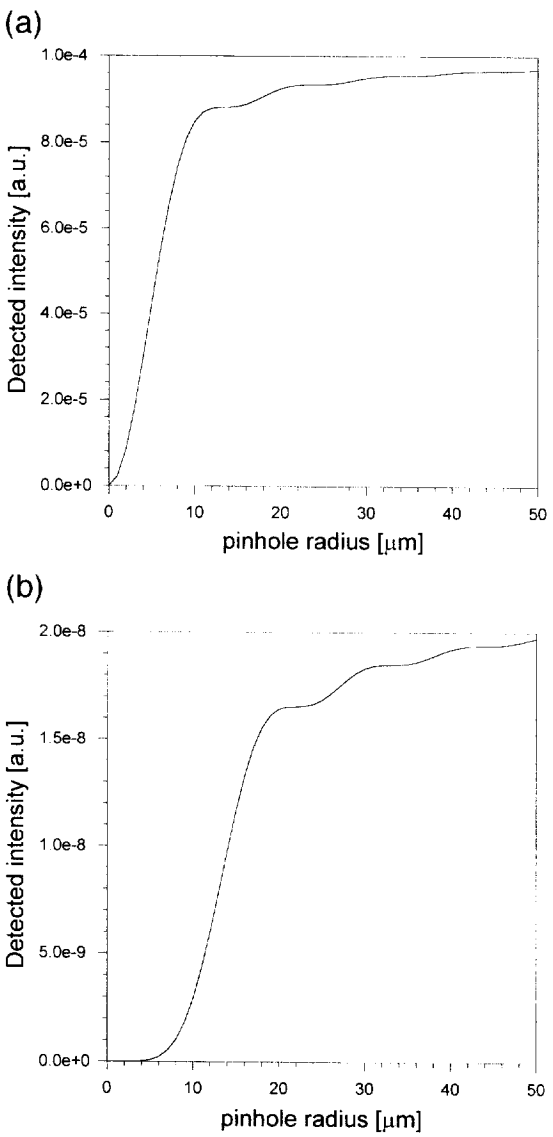

Fig. 8. Detected intensity for a linearly polarised microscope with parallel (a) and crossed (b) polarisers as a function of pinhole radius.

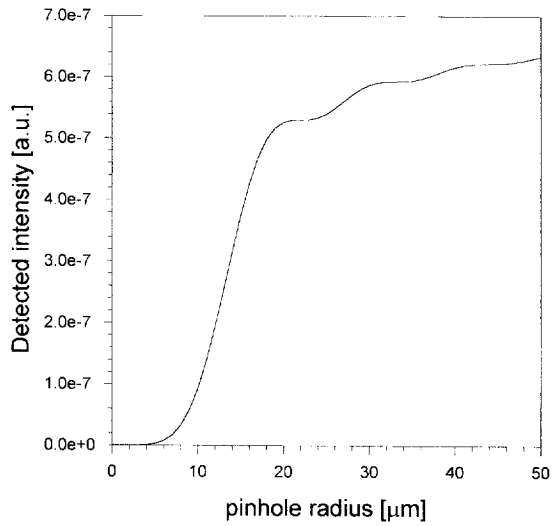

Fig. 9. Intensity of an incoherent detector for on-axis scatterer and for crossed analyser as a function of pinhole radius

$\gamma = 0°$ than for a circularly polarised set-up. The detector signals are equal for $\gamma = 45°$ and finally when $\gamma = 90°$ the circularly polarised signal is twice as high as the detector signal for the linearly polarised microscope.

When we take $R \to 0$, $P_2 = 0$ and hence the expression is dominated by P_0. This means that for parallel polarised case the above expression produces the well-known formula for encircled energy [15]. Fig. 8 shows the detected intensity for a linearly polarised microscope with incoherent detection ($R = 5$ μm) for parallel (a) and crossed (b) polarisers. The first local minima of these curves coincide with first minima of the intensity distributions in the focal plane. According to this the first minima occurs at ≈ 15 μm and ≈ 23 μm pinhole radii and for the parallel and crossed polariser cases, respectively. The radius for the parallel polarisers case results in a normalised pinhole radius of 4.5 that matches exactly the number derived by Cox and Sheppard [17]. It is, however, interesting to note that the first minimum of the crossed polarisers case occurs at a much larger radius (corresponding to a normalised pinhole radius of 6.8) that suggests that by crossing the polarisers the light distribution widens [7].

We note that for the ideal lens case, Eq. (34), as follows from Eqs. (55) and (57), the detector signal for the linearly and circularly polarised microscopes are equal for *any* analyser setting (since M_1 for the two cases are identical).

5.3. Detector signal from a point scatterer

In the following we assume that no defocus is applied when the distributions are computed for a dielectric point scatterer. It is of particular interest to calculate the signal for both coherent and incoherent detectors when the scat-

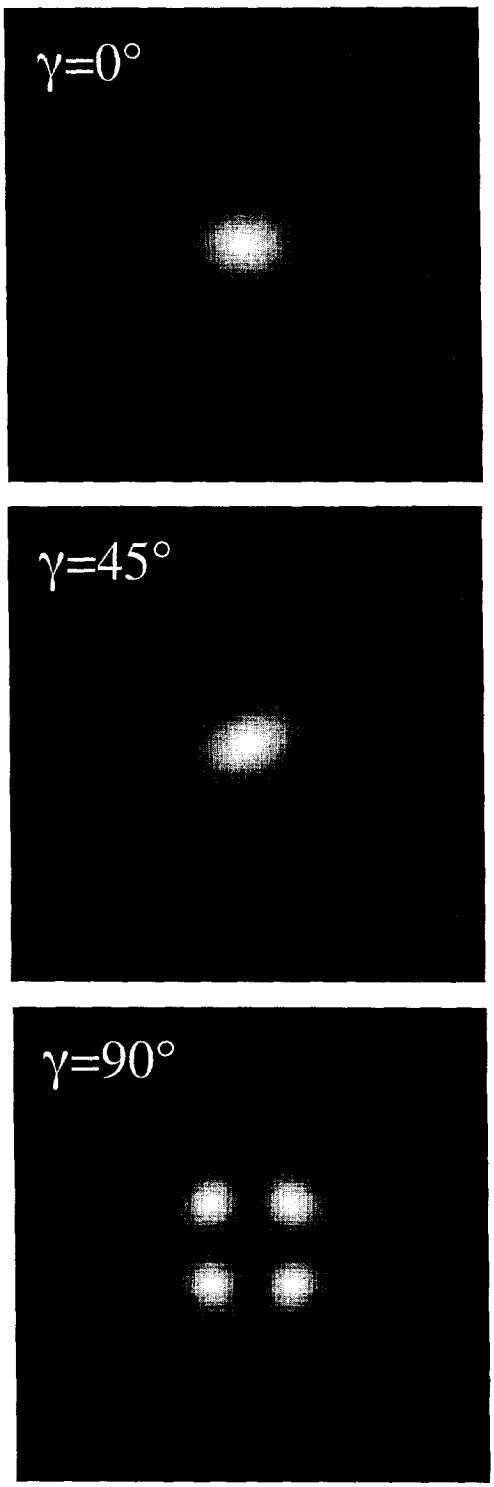

Fig. 10. Simulated images of a point scatterer obtained with a coherent detector and for $\gamma = 0°$ (a); $\gamma = 45°$ (b); $\gamma = 90°$ (c). Total image size is 2×2 μm.

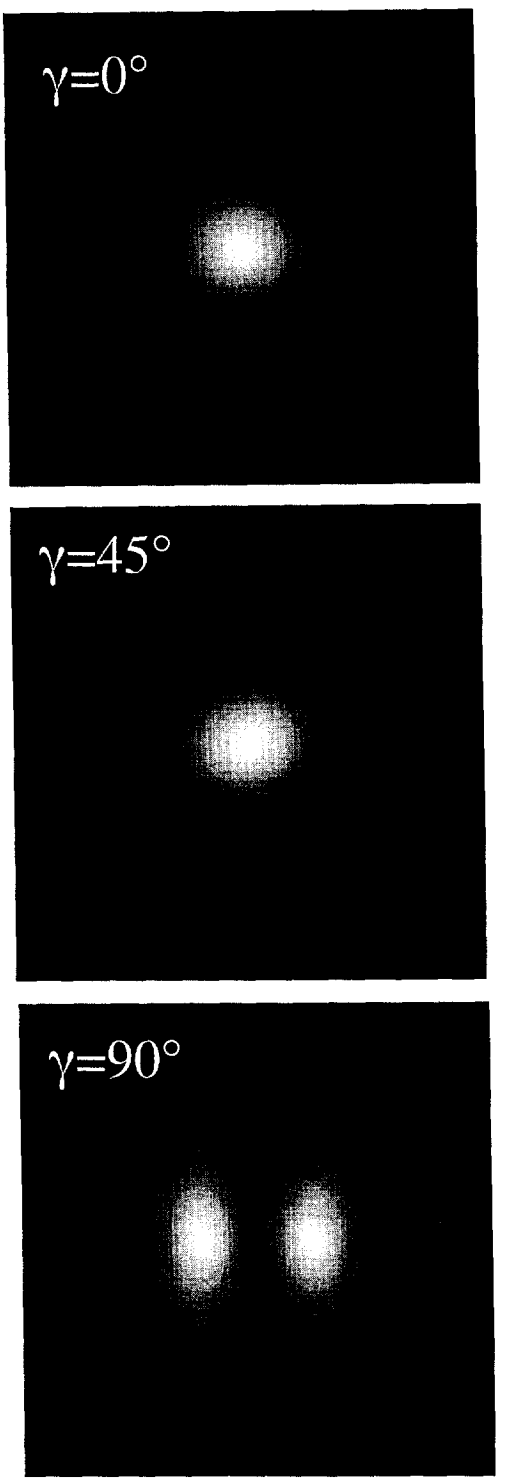

Fig. 11. Simulated images of a point scatterer obtained with an incoherent detector and for $\gamma = 0°$ (a); $\gamma = 45°$ (b); $\gamma = 90°$ (c). Total image size is 2×2 μm.

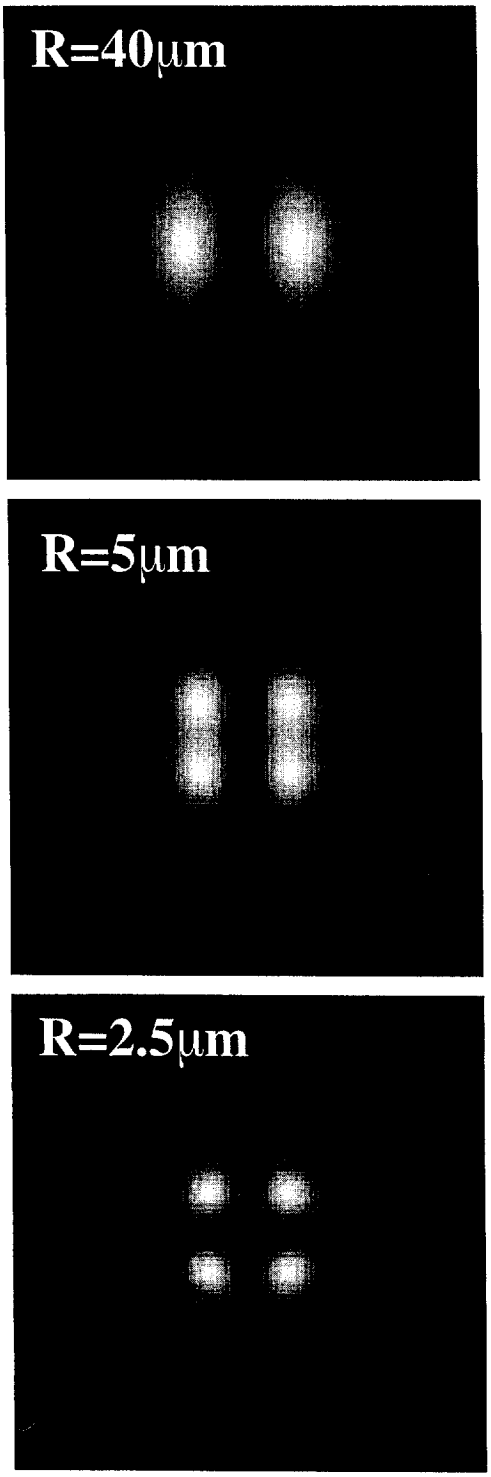

Fig. 12. Simulated images of a point scatterer obtained with a incoherent detector and for $\gamma = 90°$ with pinhole radii of $R = 40$, 5 and 2.5 μm. Total image size is 2×2 μm.

terer is located in the focus ($\rho_s = 0$) and the analyser set to crossed direction. Eq. (54) reveals that there will be zero detected signal present for a coherent detector and for $\gamma = 90°$. The signal measured by an incoherent detector, on the other hand, for $\gamma = 90°$ is given by:

$$I = \int_0^R \left(I_2^{\prime\prime} \right)^2 \rho \, \mathrm{d}\rho, \tag{59}$$

where we have ignored constant multipliers and which is plotted as a function of pinhole radius R in Fig. 9. This figure shows that the curve is similar to that obtained for the detected intensity, as a function of pinhole radius, for a linearly polarised microscope having no specimen (see Fig. 8(b)).

We have used Eq. (54) to compute the detected intensity for $R = 0$, uniform sensitivity coherent detector as a function of lateral scanning position and the results are plotted in Fig. 10a, b and c for $\gamma = 0$,45 and 90°, respectively. The distribution corresponding to $\gamma = 0°$ is slightly elliptical with a major axis coinciding with the y axis, whilst the one corresponding to $\gamma = 45°$ is slightly elliptical, with its major axis coinciding with the $y = x$ line. When the analyser is turned to the crossed position ($\gamma = 90°$) then the distribution exhibits the well-known four-leaf pattern that is in complete agreement with previous results of Wilson et al. [7].

Turning now to the case of an incoherent detector [Eq. (53)] a scatterer is laterally scanned through the focus. The results of this computation, which was obtained by using $R = 40$ μm are shown in Fig. 11a, b and c for $\gamma = 0$,45 and 90°, respectively. The distribution corresponding to $\gamma = 0°$ is slightly asymmetrical and we find again the same slight ellipticity in the distribution for $\gamma = 45°$. When the analyser is set to $\gamma = 90°$ direction the distribution possesses a one fold symmetry with respect to the axis of incident polarisation.

To illustrate the effect of the pinhole radius on the simulated images we have computed for a linearly polarised microscope and for crossed polarisers the simulated images for pinhole radii of $R = 40$, 5 and 2.5 μm, as shown in Fig. 12. The figure reveals that whilst $R = 40$ μm pinhole radius produces an incoherent detection, the $R = 5$ μm radius approaches the coherent limit and finally for $R = 2.5$ μm the distribution exhibits an almost perfect four-fold symmetry and hence the four-leaf pattern.

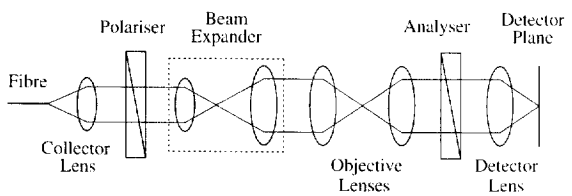

Fig. 13. Schematic diagram of the experimental arrangement for the linearly polarised microscope. The objective lenses were identical, high aperture lenses and oil immersion has been used.

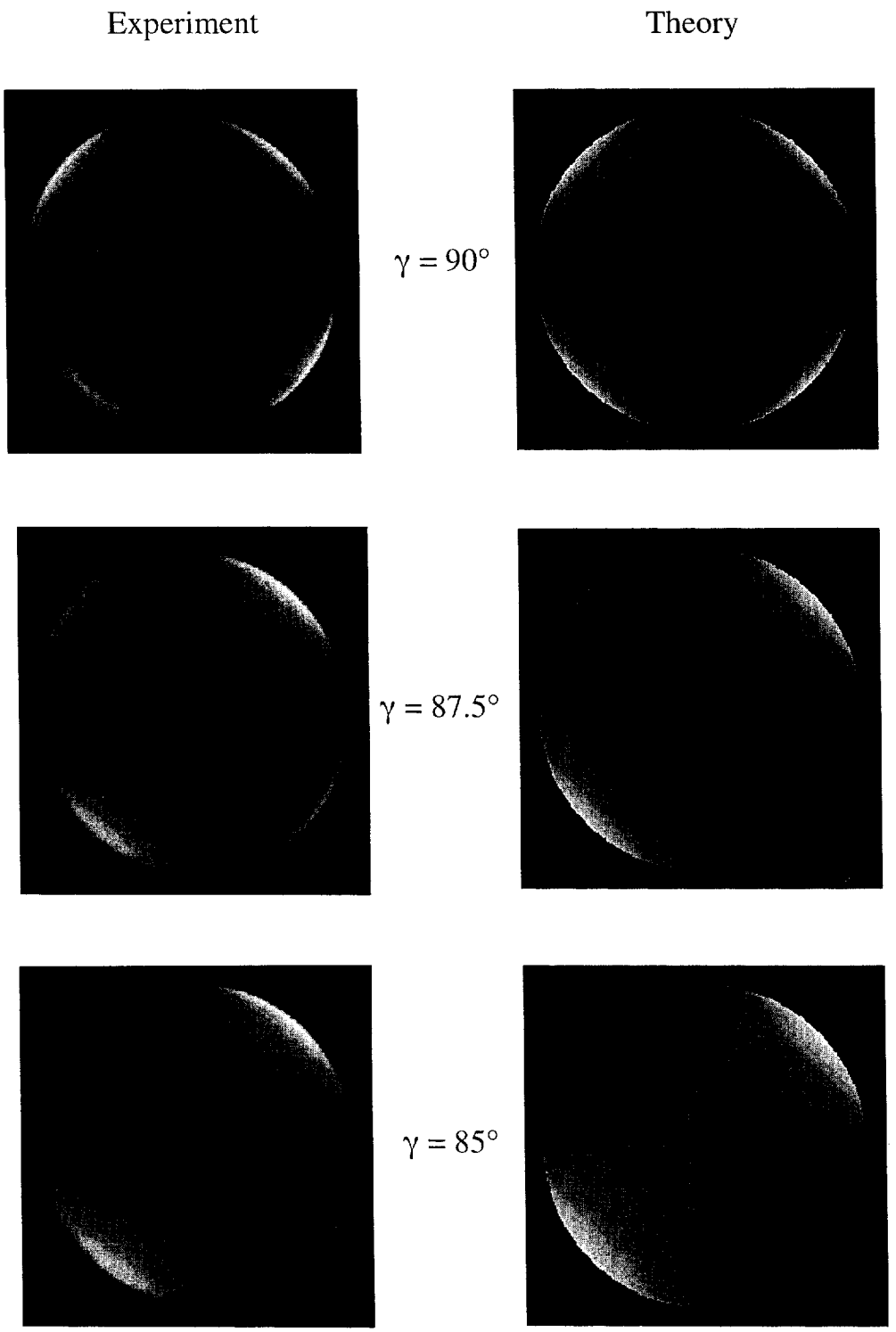

Fig. 14. Experimental and theoretical images of intensity distributions in the back focal plane of the second objective lens as functions of the analyser angle.

6. Experimental results

Schematic diagram of our experimental arrangement for a linearly polarised microscope is shown in Fig. 13. The light of a He-Ne laser ($\lambda = 632.8$ nm) was coupled in and launched from a single mode optical fibre. The light was then collimated and polarised by a Nicol prism polariser. We placed the polariser in the narrow beam diameter section of the optical arrangement because only the middle part of the polariser possesses the nominal 10^5–10^6

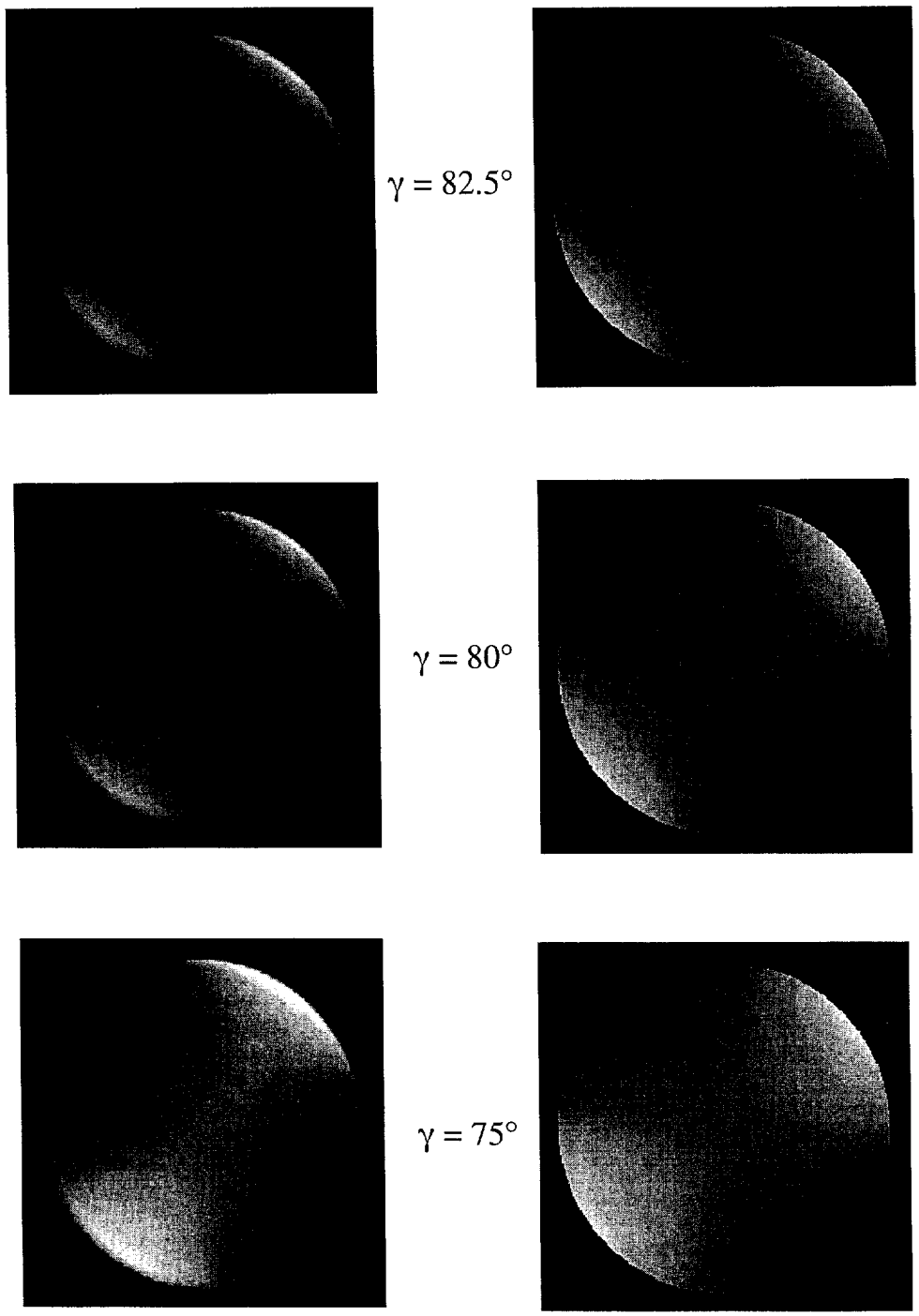

Fig. 14 (continued).

extinction. The beam was then expanded and incident upon a Leica high aperture oil immersion objective lens. An identical pair of the lens was used in a confocal configuration to recollimate the light. Immersion oil was used between the two lenses, but otherwise no specimen was placed between the two lenses. These lenses possess a numerical aperture setting ring. We have reduced the numerical aperture of both objective lenses (to NA = 1.3) in order to minimise the internal light reflection within the lenses. The light passing through and collimated by the second lens was incident upon a polariser (analyser) and is then focused by a 100 mm focal length singlet to the detector plane.

Alternatively, the detector lens was removed and the back focal plane of the second objective lens was imaged onto a CCD camera by two relay lenses. In this way we were able to record the back focal plane intensity distributions of the system with different analyser angle. The results of this measurement are shown in Fig. 14 together with theoretical predictions, as obtained from Eq. (17). The slight asymmetry in the experimental images was caused by one of the objective lenses not being centered on the optical axis. The figure shows that the assumption of a spherical interface is highly justified in our theoretical model. We have also computed the back focal plane

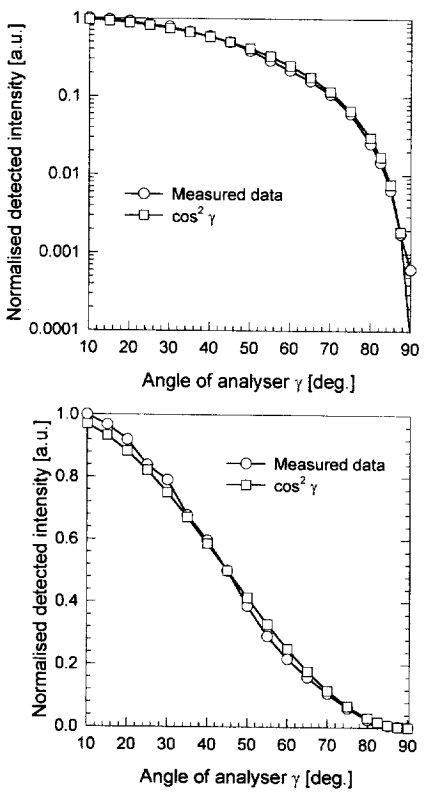

Fig. 15. Experimental and theoretical results of detected intensity as a function of analyser angle for a linearly polarised incoherent microscope.

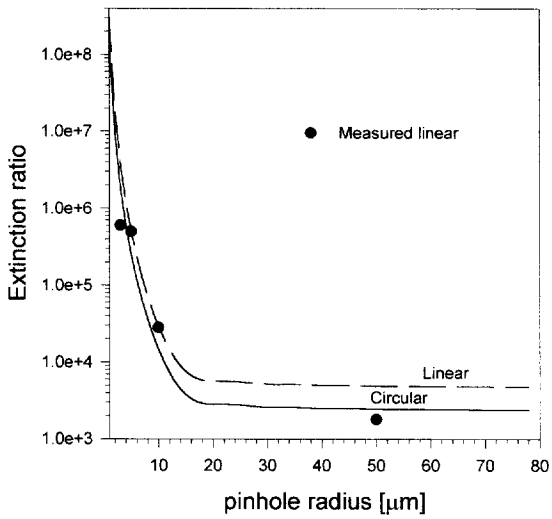

Fig. 16. Experimental and theoretical results of extinction ratio as a function of pinhole radius for linearly and circularly polarised incoherent microscopes.

distributions for a reflection type linearly polarised microscope (results are not given in this paper) and found that, for example, a gold mirror would not significantly modify the back focal plane intensity distributions.

The detected intensity was measured for a linearly polarised setup (Fig. 13) as a function of the analyser angle. The result of this measurement is shown in Fig. 15. In the same figure we have plotted the function $\cos^2\gamma$ that appears to be the major factor influencing the analyser angle dependent detected intensity. The logarithmic scale figure shows that, apart from the analyser settings that are close to the cross polar direction ($\gamma = 90°$), the function $\cos^2\gamma$ agrees well with our experimental results.

The extinction ratio was also measured for a few pinhole radii and the results are plotted in Fig. 16. We have given, for reference, the results of our theoretical predictions for a linearly and a circularly polarised microscope. This figure shows that results of our theory are in excellent agreement with those of the experiment for smaller pinhole radii. The extinction ratio for the smallest pinhole radius (2.5 μm) shows a 'saturation' effect that is due to the fact that the polarisers already reached their limit in extinction ratio, i.e. no smaller pinhole size would improve on the extinction ratio. The measured extinction ratio value for the pinhole radius of 50 μm only slightly deviates from the theoretical curve. This may well be because this pinhole size is sufficiently large to detect glare and light scattered from other optical components (e.g. due to no or poor quality anti-reflection coating).

7. Conclusions

In this paper we have presented a high aperture theory for the description of polarised light microscopes. We have

introduced the concept of high aperture ray-tracing which was found to be particularly useful for the description of polarised light microscopes. We have constructed a simple theoretical model for high aperture objective lenses that has enabled us to treat the light polarisation changes occurring at the surfaces of high aperture microscope objective lenses. We have obtained general expressions for a high aperture polarised light microscope possessing arbitrarily set Babinet-Soleil compensators. These general expressions were shown to be greatly simplified for the special cases of linearly and circularly polarised microscopes. We have presented results for detected intensity with various analyser settings and have shown that coherent microscopes have infinite extinction ratio when ideal polarisers are used. Our experimental results support the theoretical predictions.

A theoretical model was presented for high aperture polarising microscopes imaging a point scatterer. This and other results of this paper show a complete agreement with previously published results based on various approximations.

Acknowledgements

The authors acknowledge discussions with Professor L. Solymár, FRS and thank Dr. R. Juškaitis for his help with the experiment. This work was funded by the Leverhulme Trust, UK.

References

[1] S. Inoué, Exp. Cell Research 2 (1951) 513.
[2] S. Inoué, W.L. Hyde, J. Biophys. Biochem. Cytol. 3 (1957) 831.
[3] H. Kubota, S. Inoué, J. Opt. Soc. Am. 49 (1959) 191.
[4] T. Wilson, R. Juškaitis, J. Microsc. 179 (1995) 238.
[5] T. Wilson, J.B. Tan, J. Microsc. 182 (1996) 61.
[6] T. Wilson, R. Juškaitis, P.D. Higdon, J. Microsc. 187 (1997) 8.
[7] T. Wilson, R. Juškaitis, P.D. Higdon, Optics Comm. 141 (1997) 298.
[8] B. Richards, E. Wolf, Proc. Roy. Soc. London A 253 (1954) 358.
[9] P. Török, P. Varga, Z. Laczik, G.R. Booker, J. Opt. Soc. Am. A 12 (1995) 325.
[10] P. Török, T. Wilson, Optics Comm. 137 (1997) 127.
[11] P. Török, P.D. Higdon, T. Wilson, J. Mod. Optics (1997), in press.
[12] R.M.A. Azzam, N.M. Bashra, Ellipsometry and polarized light, Elsevier, Amsterdam, 1987.
[13] A. Hardy, D. Treves, J. Opt. Soc. Am. 63 (1973) 85.
[14] G.N. Watson, A treatise on the theory of Bessel functions, 2nd ed., Cambridge, 1995.
[15] M. Born, E. Wolf, Principles of Optics, 4th ed., Pergamon, Oxford, 1970.
[16] J.W. Goodman, Introduction to Fourier optics, 1st ed., McGraw-Hill, New York, 1968.
[17] I.J. Cox, C.J.R. Sheppard, J. Opt. Soc. Am. A 3 (1985) 1152.